Direct Measurement of the Equilibrium Constants of the Reaction of Formaldehyde and Acetaldehyde with HO2 Radicals

ARTICLE *in* INTERNATIONAL JOURNAL OF CHEMICAL KINETICS · MAY 2014

Impact Factor: 1.52 · DOI: 10.1002/kin.20817

4 AUTHORS:

Pranay Morajkar
Goa University
13 PUBLICATIONS **70** CITATIONS
SEE PROFILE

Coralie Schoemaecker
Université des Sciences et Technologies de …
51 PUBLICATIONS **294** CITATIONS
SEE PROFILE

Mitchio Okumura
California Institute of Technology
133 PUBLICATIONS **3,015** CITATIONS
SEE PROFILE

Christa Fittschen
CNRS - Université Lille 1
113 PUBLICATIONS **1,348** CITATIONS
SEE PROFILE

Direct Measurement of the Equilibrium Constants of the Reaction of Formaldehyde and Acetaldehyde with HO_2 Radicals

PRANAY MORAJKAR,[1] CORALIE SCHOEMAECKER,[1]
MITCHIO OKUMURA,[2] CHRISTA FITTSCHEN[1]

[1] *PhysicoChimie des Processus de Combustion et de l'Atmosphère*–PC2A, UMR 8522, *Université Lille Nord de France*, F–59650 *Villeneuve d'Ascq*, *France*

[2] *Division of Chemistry and Chemical Engineering*, *California Institute of Technology*, *Pasadena*, CA 91125, USA

Received 15 June 2013; revised 31 July 2013; accepted 1 August 2013

DOI 10.1002/kin.20817
Published online in Wiley Online Library (wileyonlinelibrary.com).

ABSTRACT: Rate and equilibrium constants for the reaction of HO_2 with formaldehyde

$$CH_2O + HO_2 \leftrightarrow HOCH_2O_2 \quad \text{(R1)}$$

and acetaldehyde

$$CH_3CHO + HO_2 \leftrightarrow CH_3CH(OH)O_2 \quad \text{(R2)}$$

have been directly measured. The concentration of HO_2 radicals was followed in a time-resolved method by coupling cw-CRDS (cavity ringdown spectroscopy) to laser photolysis. The reaction of HO_2 with CH_2O (R1) was measured at 50 Torr helium over the temperature range 292–306 K, whereas the reaction of CH_3CHO with HO_2 (R2) was measured in 50 Torr He but at only 294 K. The observed HO_2 decay profiles were modeled to take into account secondary chemistry, especially that of the reaction products, hydroxyl-peroxy radical adducts. The rate constants for forward and back reactions of (R1) at 297 K were found to be $k_1 = (3.3 \pm 0.6) \times 10^{-14}$ cm^3 molecule^{-1} s^{-1} and $k_{-1} = (55 \pm 5)$ s^{-1}, respectively, both roughly a factor of two slower than earlier measurements (possibly due to falloff effects), while the equilibrium constant was found to be $K_1 = (6.0 \pm 1.8) \times 10^{-16}$ molecule^{-1} cm^3 at 297 K, in good agreement with earlier, more

Correspondence to: Christa Fittschen e-mail: christa.fittschen@univ-lille1.fr.

indirect determinations. The equilibrium constant of the reaction with CH_3CHO was found to be $K_2 = (1.7 \pm 0.5) \times 10^{-17}$ molecule^{-1} cm^3 at 294 K, with the forward rate constant $k_2 = (1.5 \pm 0.75) \times 10^{-14}$ cm^3 molecule^{-1} s^{-1} and the rate constant for the back reaction $k_{-2} = (900 \pm 450)$ s^{-1}. © 2013 Wiley Periodicals, Inc. Int J Chem Kinet 1–15, 2013

INTRODUCTION

Formaldehyde (CH_2O) is an important intermediate in the tropospheric photooxidation of both methane and nonmethane volatile organic compounds (VOCs). It is also emitted to the troposphere both through natural and anthropogenic sources as a result of direct emission from vegetation or from the incomplete combustion of fossil fuels and biomass. In the troposphere, the most important, well-known removal pathways are photolysis by solar radiation and its oxidation by OH radicals. In addition to this, the reaction of CH_2O with HO_2 radicals has been a subject of research interest for many years, because—especially under low NO_x conditions and at low temperatures—the title reaction can contribute to the loss of CH_2O from the troposphere as well as influence the HO_2 radical budget of the troposphere. However, the reaction is more important in laboratory experiments, where the CH_2O concentrations are typically much higher than found in the atmosphere.

The reaction of CH_2O and HO_2 leads through a sequence of two equilibrium reactions to the formation of the hydroxymethyl peroxy radical ($HOCH_2O_2$):

$$HO_2 + CH_2O \leftrightarrow HO_2 - CH_2O \qquad \text{(R1a)}$$

$$HO_2 - CH_2O \leftrightarrow HOCH_2O_2 \qquad \text{(R1b)}$$

This overall equilibrium (R1a + b) was first studied by Su et al. [1] in 1979 and Niki et al. [2] in 1980. They investigated the Cl atom–initiated oxidation of CH_2O in a large photoreactor, coupled to a detection of reaction products by FTIR. They also investigated the subsequent reaction of $HOCH_2O_2$ with HO_2 radicals, leading to the formation of α-hydroxy-methylhydroperoxide ($HOCH_2OOH$):

$$HO_2 + HOCH_2O_2 \rightarrow HOCH_2OOH + O_2 \qquad \text{(R3a)}$$

The reaction of CH_2O with HO_2 was later investigated by Veyret et al. [3], who flash photolyzed a mixture of CH_2O, O_2, and NO and monitored the rate and yield of NO_2 appearance. They fitted the NO_2 formation yield and rate to a complex model to obtain the rate constants for the equilibrium reaction of HO_2 radicals with CH_2O in a rather indirect way. In 1985, Barnes et al. [4] studied the title reaction in a large photoreactor at 273 K in the presence of NO_2. They monitored the reactants and their products by FTIR absorption spectroscopy. They provided more evidence for the formation of the $HOCH_2O_2$ radical as the primary reaction product of the reaction between CH_2O and HO_2 by the IR spectroscopic identification of its NO_2 recombination product, $HOCH_2OONO_2$. Simulation of the concentration–time profiles of HO_2NO_2, H_2CO, and $HOCH_2OONO_2$ led to the rate constant for reaction (R1) as $k_1 = (1.1 \pm 0.4) \times 10^{-13}$ cm^3 molecule^{-1} s^{-1} and $k_{-1} = 20$ s^{-1} at 273 K. The equilibrium constant was also investigated by Zabel et al. [5] in 1987 in the temperature range 283–373 K: They photolyzed in a gas flow system a mixture of $CH_2O/O_2/N_2$ and analyzed the condensable reaction products after cryotrapping on a cold finger at 96 K. HO_2 and $HOCH_2O_2$ were quantified by ESR spectroscopy, and an equilibrium constant of $K_1 = 3.4 \times 10^{-15}$ molecule^{-1} cm^3 at 298 K was obtained. However, this study was based on the measurement of product yields and no time-resolved measurements were performed. Morrison and Heicklen [6] extracted a rate constant for the forward reaction of the equilibrium (R1) from fitting stable products following the photolysis of CH_2O in the presence of NO_2.

In 1989, Veyret et al. [7] reinvestigated the reaction of HO_2 with CH_2O using flash photolysis coupled to time-resolved UV absorption spectroscopy. In this study, the HO_2 radicals were generated by flash photolyzing a $Cl_2/CH_2O/O_2$ mixture. These measurements provided the first UV absorption spectrum of $HOCH_2O_2$ radicals in the wavelength range 200–270 nm. Simulations of the HO_2 concentration time profiles were performed from which the rate and equilibrium constants $k_1 = 6.31 \times 10^{-14}$ cm^3 molecule^{-1} s^{-1}, $k_{-1} = 125.7$ s^{-1}, and $K_1 = 4.99 \times 10^{-16}$ molecule^{-1} cm^3 at 298 K were determined. However, UV absorption spectroscopy is not very selective for simultaneously detecting both the HO_2 and $HOCH_2O_2$ radicals, because both species have large and unstructured bands in the same wavelength region. Relatively high initial radical concentrations were used in this study ($[HO_2]_0$ up to 1×10^{14} cm^{-3}) to be sensitive to the subsequent reaction of HO_2 radicals with the adduct (R3a). Also, high CH_2O concentrations ($(1–9) \times 10^{16}$ cm^{-3}) were used, leading to kinetic decays for the initial reaction on the timescale of less

than 1 ms. In 2005, Hermans et al. performed density functional theory calculations on this reaction and computed thermal rate constants using transition state theory (high-pressure limit) [8]. They calculated an equilibrium constant at 300 K of $K_1 = 1.6 \times 10^{-15}$ molecule^{-1} cm^3 and rate coefficients of $k_1 = 3.2 \times 10^{-13}$ cm^3 molecule^{-1} s^{-1} and $k_{-1} = 200$ s^{-1} in the high-pressure limit. Improved energetics of the adduct have been obtained from more recent higher level calculations [9]. Very recently, calculation on the structure and the spectroscopy of the peroxy radicals have been performed by Delcey et al. [10]. Formation of the hydroxy-methyl radical from $HO_2 + CH_2O$ has been verified by direct detection of the vibrational and electronic spectra using infrared and near-infrared cavity Ringdown spectroscopy [11], though no kinetics of the reaction was reported.

In 1989, Burrows et al. [12] proposed that the reaction of HO_2 with $HOCH_2O_2$ directly leads to the formation of HCOOH even in the absence of NO and have reported a product branching ratio of 60 ± 15% for (R3a) and 40 ± 15% for (R3b), respectively:

$$HOCH_2O_2 + HO_2 \rightarrow HCOOH + H_2O + O_2 \quad \text{(R3b)}$$

Recently, Jenkin et al. [13], while investigating the same reaction, identified a reaction channel generating OH radicals, assuming the oxy radical $HOCH_2O$ and O_2 as coproducts:

$$HOCH_2O_2 + HO_2 \rightarrow OH + HOCH_2O + O_2 \quad \text{(R3c)}$$

They concluded from the same study that the oxy radical would react subsequently with O_2 to exclusively form HO_2 and HCOOH; this reaction would explain the formic acid production observed in the earlier studies [1,2,4,12,13]:

$$HOCH_2O + O_2 \rightarrow HCOOH + HO_2 \quad \text{(R4)}$$

They reported a yield of 20 ± 5% for the radical pathway (R3c), along with 30 ± 6% and 50 ± 11% for (R3b) and (R3a), respectively.

In 2010, Nguyen et al. [14] performed theoretical calculations and provided evidence for the existence of another channel generating OH radicals. The cross-reaction of $HOCH_2O_2$ with HO_2 was found to proceed via a short-lived unstable tetroxide, which subsequently decomposes via two different channels:

$$HOCH_2O_2 + HO_2 \rightarrow HOCH_2O_4H \rightarrow HCOOH + O_2 + H_2O \quad \text{(R3d)}$$

$$\rightarrow HCOOH + HO_2 + OH \quad \text{(R3e)}$$

Interestingly, they predicted that formic acid could be produced in two different channels whereas OH radicals were produced in only one, as shown in reaction channels (R3d) and (R3e). Reaction (R3e) was found to be twice as slow as reaction (R3d).

Acetaldehyde is another oxygenated VOC that is ubiquitous in the troposphere. In a very recent study [15], average annual concentrations of 428 ± 190 ppt are found for CH_3CHO in the tropical remote marine boundary layer between 2006 and 2011. These authors have compared their results with the global CAM-Chem model [16] and have found that the CH_3CHO concentration is underestimated by a factor of 10, rising to as large as 40 during summer. These discrepancies indicate that the sources and sinks of acetaldehyde are still not well understood. The main degradation pathway of acetaldehyde is a reaction with OH radicals: The rate constant is 1.5×10^{-11} cm^3 molecule^{-1} s^{-1}, i.e., around two times faster than the reaction of formaldehyde [17], whereas its absorption cross sections in the actinic range are smaller compared to those of CH_2O.

Moortgat et al. [18] first proposed the reaction of CH_3CHO with HO_2:

$$HO_2 + CH_3CHO \leftrightarrow CH_3CH(OH)O_2 \quad \text{(R2)}$$

by analogy with the reaction of CH_2O, to reproduce the observed concentrations of acetic acid, which would be formed through the subsequent reactions of the initial hydroperoxy radical with O_2. Since then, the equilibrium has been experimentally explored by Crawford et al. [19] and Tomas et al. [20]. These studies agree on the approximate value of the equilibrium constant: $K_2 \approx 2 \times 10^{-17}$ cm^3 molecule^{-1} at 298 K; however, there is a large disagreement over the rate constants of the association reaction of $CH_3CHO + HO_2$ (k_2) and the back dissociation reaction (k_{-2}). Moortgat et al. [18] first estimated k_2 by quantifying the products of the CH_3CHO photolysis using FTIR and UV spectroscopy. They reported $k_2 = 1 \times 10^{-15}$ cm^{3}molecule^{-1} s^{-1} assuming $k_{-2} = 100$ s^{-1} based on the yield of CH_3COOH. Contradicting the above results, in 1999 Crawford et al. [19] estimated $k_2 = 5 \times 10^{-14}$ cm^3 molecule^{-1} s^{-1}. In 2001, Tomas

et al. [20] reported another investigation of the title reaction that was carried out by flash photolysis coupled to time-resolved UV absorption spectroscopy. They determined an equilibrium constant of $K_2 = 3.2 \times 10^{-17}$ cm^3 molecule^{-1} and rate constants of $k_2 = 4.4 \times 10^{-14}$ cm^3 molecule^{-1} s^{-1} and $k_{-2} = 1365$ s^{-1} at 294 K. More recently, Moortgat et al. [21] used the rate and equilibrium constants obtained by Tomas et al. to explain the yields of stable products observed by gas chromatography following the photolysis of CH_3CHO at different wavelengths. They obtained better agreement between model simulation and experimental results if they decreased the rate constant for the forward reaction to $k_2 = 1.5 \times 10^{-14}$ cm^{3}molecule^{-1} s^{-1} and the equilibrium constant to $K_2 = 1 \times 10^{-17}$ cm^3 molecule^{-1}. In their 2005 paper, Hermans et al. also calculated the rate and equilibrium constants for reaction (R2) [8]. They found at 298 K an equilibrium constant of $K_2 = 9.5 \times 10^{-17}$ cm^{-3} and computed rate constants at 1 atm (and assuming a small 0.94 correction due to pressure falloff) of $k_2 = 2 \times 10^{-13}$ cm^3 molecule^{-1} s^{-1} and $k_{-2} = 2130$ s^{-1}, in fairly good agreement with the results of Tomas. They estimated that in the upper troposphere/lower stratosphere, the equilibrium formation of an acetaldehyde adduct was too slow to compete with OH oxidation of acetaldehyde.

In this paper, we present a new investigation of the equilibrium reactions of HO_2 with both formaldehyde and acetaldehyde, using a direct approach: Concentration–time profiles of HO_2 radicals are directly measured in the presence of CH_2O and CH_3CHO using the highly sensitive, selective, and absolute technique of cw-cavity ring down spectroscopy (cw-CRDS) coupled to laser photolysis.

EXPERIMENTAL

All experiments were performed by coupling laser photolysis of precursors with time-resolved detection of HO_2 radicals by cw-CRDS in the near IR. A detailed description of the experimental setup has already been published [22,23] and will therefore not be given here. We recently improved the acquisition system, as described by Votava et al [24]: A microcontroller-based unit tracked the piezo crystal and increased the rate of cw-CRDS events, thus enhancing the signal-to-noise ratio. All data were acquired using an acquisition card (National Instruments PC-6259) installed in a personal computer, and all programs were written in Labview, version 8.2.1. Briefly, the photolysis cell had three axes and was made of stainless steel, internally coated with Teflon. Photolysis was achieved along the longest axis with an excimer laser (Lambda Physik LPX 202i) operating at 248 nm. The beam entering the cell through a quartz window had a size of approximately 1.5×3.0 cm^2, with a fluence of around 50 mJ cm^{-2}.

In addition, time-resolved detection of OH radicals by high repetition rate laser-induced fluorescence (LIF; operated at 10 kHz) has been used in a few experiments to accurately quantify the CH_3CHO concentration in the glass bulbs to unravel possible polymerization of CH_3CHO after preparation of the mixtures. The excitation beam entered the cell through a quartz window, located at 90° with respect to the photolysis laser, and the fluorescence was collected at 90° with respect to the plane defined by the two laser beams. The principle has been described in detail in an earlier work [25] and will not be repeated here.

Cw-CRDS was synchronized to the laser photolysis pulse to obtain time-resolved profiles of the absolute HO_2 radical concentration following the photolysis of CH_2O or CH_3CHO in the presence of O_2. The mirrors (Los Gatos) used in this work had a reflectivity of $R \approx 0.999954$, leading to ring down times in the empty cavity of around 60 μs. In some experiments, H_2O_2 was added to the reaction mixture by bubbling a fraction of the helium flow through a 50% solution of H_2O_2 to increase the initial radical concentration. HO_2 radicals were detected by absorption at 6638.20 cm^{-1}, the center of the strongest line in the $2\nu_1$ band [26]. Absolute concentrations of [HO_2] were determined from the known cross section of this absorption. Cw-CRDS was also employed as a spectroscopic method, independent of laser photolysis, for the measurement of absolute CH_2O concentrations present in the photolysis cell [25].

Different concentrations of CH_2O were produced in a continuous manner by gently depolymerizing paraformaldehyde that was kept in a trap whose temperature was maintained by a water bath. The depolymerized, gaseous CH_2O was transported directly to the photolysis cell by flushing a small flow of He (100 cm^3 min^{-1} STP) through the trap. To minimize the repolymerization of the CH_2O monomer, the small flow was mixed directly at the exit of the trap with the main He flow (400 cm^3 min^{-1} STP). No deposition of repolymerized CH_2O was visible within the short Teflon tubes that connected the trap and the photolysis reactor (≈50 cm). The amount of CH_2O reaching the photolysis cell strongly depended on the temperature of the water bath: concentrations between 3 and 7×10^{15} cm^{-3} were obtained by varying the bath temperature between 323 and 343 K. The CH_2O concentration

within the photolysis reactor was directly monitored by cw-CRDS. We have recently measured absolute absorption cross sections for several lines of CH_2O in the wavelength range near the current HO_2 absorption line [25]. These measurements were based on measuring pseudo–first-order decays of OH radicals in the presence of different concentrations of CH_2O: From the well-known rate constant of the reaction between CH_2O and OH, the absolute concentration of CH_2O can then be deduced. These absorption cross sections were used in the present work to quantify in situ the CH_2O concentration. In the beginning of an experiment, the temperature of the water bath and all flows were set to the desired values and the wavelength of the distributed feedback (DFB) laser was set at the center of the CH_2O absorption line at 6625.248 cm^{-1}. Once the CH_2O concentration within the reactor was stable, the concentration was determined by scanning the full absorption line. The absolute CH_2O concentration within the reactor was determined from the known absorption cross section (2.47×10^{-22} cm^2 at 50 Torr) [25].

Acetaldehyde (CH_3CHO) was prepared as a diluted mixture (up to 5%) in darkened bulbs. Different concentrations within the photolysis cell were then obtained by mixing different flows, measured by calibrated flowmeters, into the main helium flow. Since acetaldehyde could possibly polymerize within the bulb, the concentration of the bulb was checked periodically by cophotolyzing H_2O_2 with a known concentration of CH_3CHO, calculated from the different flows: The subsequent decay of OH radicals was governed by its reaction with CH_3CHO, and the CH_3CHO concentration could be retrieved from the known rate constant [17] and compared with the concentration computed from measuring the different flows and the pressure. No discrepancy with the calculated CH_3CHO concentration was ever observed, indicating that polymerization of CH_3CHO was negligible in our system.

All experiments were conducted at a total pressure of 50 Torr helium (Alpha Gas; 5.0). The temperature was varied through electrical heating of the insulated reactor; the temperature was measured by a thermocouple in the center of the reaction zone. Concentrations have been varied typically between CH_2O (3–7) $\times 10^{15}$ cm^{-3}, CH_3CHO: (1–3) $\times 10^{16}$ cm^{-3}, O_2: (0.2–30) $\times 10^{16}$ cm^{-3} for CH_3CHO experiments, 15×10^{16} cm^{-3} for CH_2O experiments, H_2O_2: (1–2) $\times 10^{14}$ cm^{-3}, and initial HO_2: (0.7–4) $\times 10^{12}$ cm^{-3}. All flows were controlled by calibrated flowmeters. He (6.0%; Praxair) was used directly. Para-formaldehyde (Aldrich; 95%), CH_3CHO (Aldrich; ≥99.5%), and H_2O_2 (Aldrich; 50%) were used without further purification.

RESULTS

Generation of HO_2 Radicals

HO_2 radicals were generated by 248-nm pulsed laser photolysis of the aldehydes. The photolysis of CH_2O forms H atoms and HCO radicals with a quantum yield of $\phi = 0.3$ [27]. Quantum yields for acetaldehyde at 248 nm are not precisely known, but yields on the same order of magnitude ($\Phi_H \approx 0.1$ and $\Phi_{HCO} \approx 0.3$) can be extrapolated from Moortgat et al. [21]. Both H and HCO radicals were converted under our conditions into HO_2 radicals with pseudo–first-order rate constants of $k_5' = 7.8 \times 10^5$ s^{-1} [17] and $k_6' = 1336$ s^{-1}, respectively [28],

$$HCO + O_2 \rightarrow HO_2 + CO \qquad (R5)$$

$$H + O_2(+M) \rightarrow HO_2(+M) \qquad (R6)$$

A possible reaction of H atoms with CH_2O ($k_{300K} = 5.72 \times 10^{-14}$ cm^3 $molecule^{-1}$ s^{-1} [29], leading to $k' \approx 350$ s^{-1}) would not play any role, because the product HCO would react rapidly in (R5), whereas the stable product H_2 has no influence on the reactivity. The absorption cross section [17] of CH_3CHO at 248 nm is 9.73×10^{-21} cm^2 and led with typical initial concentrations of $[CH_3CHO] = (2–3) \times 10^{16}$ cm^{-3} to initial HO_2 concentrations of up to $[HO_2]_0 \approx (2–4) \times 10^{12}$ cm^{-3}: Such HO_2 concentrations could be detected with high signal-to-noise ratios. In the formaldehyde experiments, the HO_2 concentration generated solely by CH_2O photolysis was too low, both because the absorption cross section of CH_2O at 248 nm is lower ($\sigma = 2.53 \times 10^{-21}$ cm^2) and because the CH_2O concentrations that we typically used were lower (up to 7×10^{15} cm^{-3}): Typical conditions ($[CH_2O] = 5 \times 10^{15}$ cm^{-3}, $E_{248nm} = 50$ mJ cm^{-2}) led to $[HO_2]_0 \approx 3 \times 10^{11}$ cm^{-3}. Therefore, H_2O_2 was cophotolyzed in most CH_2O experiments to increase the HO_2 concentration: H_2O_2 was added by saturating a small fraction of the main He flow with H_2O_2 prior to mixing with the CH_2O flow by bubbling through a trap containing a 50% H_2O_2/H_2O solution. Its photolysis at 248 nm ($\sigma = 9.1 \times 10^{-20}$ cm^2) led to two OH radicals [30] that were each subsequently converted to one HO_2 radical by a reaction with either H_2O_2 or CH_2O:

$$OH + CH_2O \rightarrow HCO + H_2O \qquad (R7)$$

$$OH + H_2O_2 \rightarrow HO_2 + H_2O \qquad (R8)$$

Under typical experimental conditions ($[H_2O_2] = 1.4 \times 10^{14}$ cm^{-3}, $E_{248nm} = 50$ mJ cm^{-2}), an additional

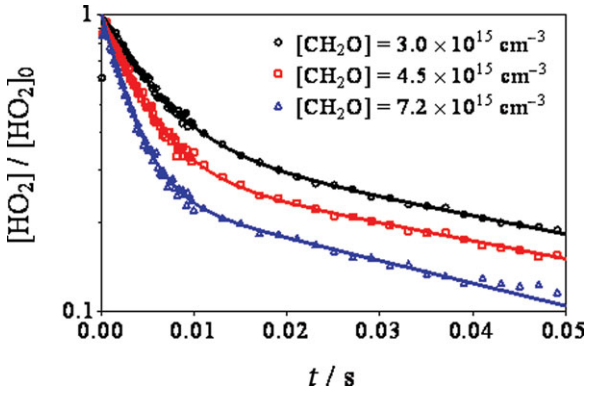

Figure 1 Normalized HO_2 decay profiles as a function of CH_2O concentration at 51 Torr total pressure, 297 K, and photolysis fluence 76 mJ cm^{-2}. Absolute, initial HO_2 concentrations were 2.0/2.5/2.7 × 10^{12} cm^{-3} for the lowest to highest CH_2O concentration. Full lines represent fits to biexponential decay.

OH concentration of around 1.7 × 10^{12} cm^{-3} was generated, reacting predominantly through (R7): The pseudo–first-order rate constant $k_7' \approx 2.6 \times 10^4$ s^{-1} was much faster than the reaction with H_2O_2 ($k_8' \approx 238$ s^{-1}).

Equilibrium Constant for the Reaction of HO_2 with CH_2O

Typical HO_2 concentration–time profiles in the presence of different CH_2O concentrations are shown in Fig. 1; for better comparison, the individual signals have been normalized to the initial HO_2 concentration. After a nearly immediate rise of the HO_2 concentration due to reactions (R5) to (R8), biexponential decays are observed. The first, fast decay can be interpreted as an approach of the HO_2 concentration to the equilibrium value defined by K_1, whereas the slower second decay is associated with a loss of HO_2 radicals through processes such as diffusion of HO_2 out of the observation volume and secondary reactions such as (R3). From such experiments, i.e., the observation of the overall loss of HO_2 radicals through establishing the equilibrium (R1), it is not possible to distinguish between (R1a) and (R1b). In a recent work on the possible corresponding equilibrium reaction between acetone and HO_2 radicals [31,32], experimental evidence has been found that only the corresponding complex formation (R1a) takes place and that the subsequent rearrangement (R1b) to formation of the peroxy radical is too slow. In the case of CH_2O, however, the fast establishment of the equilibrium (R1b) is supported from earlier experiments by end-product studies [1,2], ESR detection of the $HOCH_2O_2$ radicals [5] as well as UV-absorption studies [7]. Finally, Sprague et al. [11] have directly detected the peroxy radical $HOCH_2O_2$ by IR and near IR spectroscopy and have found that the appearance rate from the reaction is consistent with direct formation by reaction (R1b). The experimental results are consistent with calculations, which indicate that the barrier for reaction (R1b) is high in the case of acetone [33,34], but much lower than the energy of the initial reactants, $HO_2 + CH_2O$, in the case of formaldehyde [8,9]. Therefore, we have evaluated our experimental data by considering a single equilibrium reaction.

The HO_2 profiles behave as expected for an equilibrium reaction: With increasing CH_2O concentration, the HO_2 decay becomes faster and the final equilibrium concentration of HO_2 decreases. The equilibrium constant for (R1) can be written in terms of concentration as

$$K_1 = \frac{[HOCH_2O_2]_{eq}}{[CH_2O]_{eq} \times [HO_2]_{eq}} \tag{1}$$

where the concentration of CH_2O can be considered unchanged, i.e., $[CH_2O]_{eq} = [CH_2O]_0$. Neglecting any secondary reactions other than those leading to the slow second decay, a least-squares fit of the HO_2 signals to a biexponential decay will allow in principle the determination of the equilibrium constant:

$$[HO_2] = [HO_2]_0 \times F_{fast} \exp(-k_{fast} t) + [HO_2]_0 \times (1 - F_{fast}) \exp(-k_{slow} t) \tag{2}$$

with F_{fast} being the fraction of the HO_2 decay due to the fast decay. The equilibrium concentrations $[HOCH_2OO]_{eq}$ and $[HO_2]_{eq}$ can be expressed in terms of F_{fast} and the initial HO_2 concentration (extrapolated back to $t = 0$ s):

$$[HOCH_2OO]_{eq} = [HO_2]_0 \times F_{fast} \tag{2a}$$

and

$$[HO_2]_{eq} = [HO_2]_0 \times (1 - F_{fast}) \tag{2b}$$

Hence, Eq. (1) can be expressed as

$$K_1 = \frac{F_{fast}}{[CH_2O]_0 \times (1 - F_{fast})} \tag{3}$$

and only the absolute $[CH_2O]$ concentration is needed for calculating the equilibrium constant.

From such a fit, shown as full lines in Fig. 1, one can also extract the rate constants for forward and

backward reactions. The equilibrium constant can also be expressed in terms of rate constants as

$$K_1 = \frac{k_1}{k_{-1}} \tag{4}$$

The decay rate k_{fast} from the biexponential fit to Eq. (2) is equal to

$$k_{fast} = k_1 \times [CH_2O] + k_{-1} \tag{5}$$

Replacing k_{-1} in Eq. (5) by Eq. (4) and knowing K_1 from Eq. (3) allows obtaining the value for the rate constant of the forward reaction k_1:

$$k_1 = \frac{k_{fast}}{[CH_2O]_0 + (K_1)^{-1}} \tag{6}$$

The rate constant for the backward reaction k_{-1} can then be calculated directly from Eq. (4).

The biexponential fits of the three HO_2 decay profiles for the example shown in Fig. 1 returned the following fitted parameters (from the lowest to highest CH_2O concentration): $k_{fast} = (177 \pm 8)/250/346\ s^{-1}$, $k_{slow} = (13.3 \pm 1.3)/14.6/15.6\ s^{-1}$, $F_{fast} = (0.642 \pm 0.017)/0.694/0.750$ (errors are statistical only (95% confidence interval) and are shown for clarity for the first value only as they are similar for all measurements). These results can be converted into equilibrium and rate constants using the known CH_2O concentrations and the above equations: $K_1 = (6.02 \pm 0.6)/5.04/4.17 \times 10^{-16}$ molecule^{-1} cm^3, $k_1 = (3.81 \pm 0.4)/3.86/3.60 \times 10^{-14}$ cm^3 molecule^{-1}, s^{-1} and $k_{-1} = (63 \pm 6)/77/87\ s^{-1}$. While the values for k_1 are the same within the uncertainty, the fitted values of the equilibrium constant and concomitantly the rate constant of the backward reaction, k_{-1}, appear to depend on the CH_2O concentration. The apparent HO_2 equilibrium concentration increases with increasing initial radical and/or CH_2O concentration. This trend has been systematically observed in all measurements.

To be sure that the observed decay signals were purely due to HO_2 radicals, experiments were performed by tuning the detection wavelength off any HO_2 absorption line so as to observe the possible absorption due to unknown species formed after the photolysis pulse (offline signal). However, no absorption signal was observed, confirming that the recorded decay profiles were specific to HO_2 absorption and free of any signal due to other species absorbing at the detection wavelength.

In the experiments in Fig. 1, both CH_2O and initial HO_2 concentration were varied. To identify the cause of the deviations in K_1 and k_{-1}, experiments were performed with identical CH_2O/H_2O_2 concentrations but different photolysis energies. Figure 2 shows HO_2 decays with the photolysis fluence varied between 33 and 75 mJ cm^{-2}. Again, the initial HO_2 concentrations have been normalized. Although the HO_2 decays appear very similar for different photolysis energies, fits of the biexponential decays always reveal the same systematic trend in the equilibrium constant. In the example in Fig. 2, as the photolysis energy is increased, the values for F_{fast} decrease from 0.785 ± 0.005 to 0.775 ± 0.006 to 0.758 ± 0.012 (error bars are again statistical only), leading to an apparent decrease in the equilibrium constant ($5.06/4.78/4.36 \times 10^{-16}$ molecule^{-1} cm^3) with increasing initial radical concentration. The loss of HO_2 radicals at long reaction times also becomes slightly faster as the initial radical concentration is raised: k_{slow} increases from 11.3 ± 2.1 to 12.7 ± 0.8 to 15.6 ± 0.7 as the photolysis energy increases. The trends in these experiments are therefore the same as in the experiments shown in Fig. 1, in which $[CH_2O]$ (and indirectly the radical concentration) was varied.

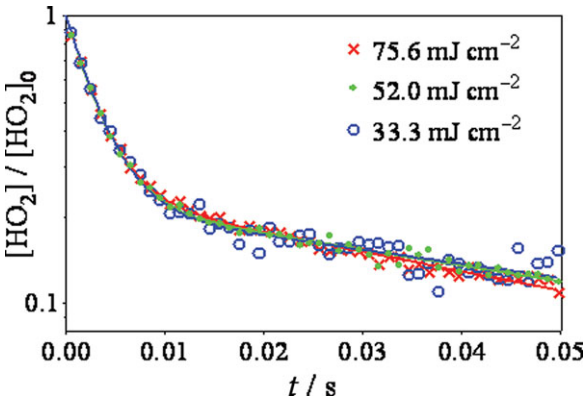

Figure 2 HO_2 concentration–time profiles as a function of photolysis laser fluence at 51 Torr, 297 K, and $[CH_2O] = 7.2 \times 10^{15}$ cm^{-3}. Signals have been normalized by the photolysis fluence for better comparison: $[HO_2]_0 = 2.68$, 2.04, and 1.34×10^{12} cm^{-3}.

We hypothesize that this systematic trend in the apparent equilibrium constants with the radical concentration is due to secondary chemistry that has not been taken into account by the simple model described above. Likely candidates for such reactions are the radical–radical reactions of the peroxy radicals, $HO_2 + HOCH_2O_2$ (reaction (R3)) and $HOCH_2O_2 + HOCH_2O_2$. The branching ratio between chain termination and radical-forming pathways can in principle affect the observed concentrations of HO_2.

In the $HO_2 + HOCH_2O_2$ reaction, the radical-forming pathway (R3c) leads ultimately to the formation of two new HO_2 radicals, i.e., the full recycling

of hydroperoxy radicals. The yield of this pathway has been estimated by Jenkin et al. [13] to be 20% and by Nguyen et al. [14] to be 15% of the total. The remaining 80 or 85% of the channels terminate the radical chain reaction and lead to loss of radicals. Because this reaction is second order in radical concentrations and is predominantly chain terminating, it will contribute to a net loss of HO_2 radicals at longer timescales and can account for some of the observed increase in k_{slow} with increasing radical concentration. However, if the radical concentrations are sufficiently high, then this reaction could be nonnegligible on the timescale for establishing the equilibrium (R1) and would then have an impact on the apparent HO_2 equilibrium concentration at shorter times.

Another candidate is the self-reaction of the adduct. Burrows et al. [12] identified two pathways:

$$2HOCH_2O_2 \rightarrow HCOOH + CH_2(OH)_2 + O_2 \quad \text{(R9a)}$$

$$\rightarrow 2HOCH_2O + O_2 \quad \text{(R9b)}$$

with an overall rate coefficient $k_9 = 6.06 \times 10^{-12}$ cm^3 molecule^{-1} s^{-1} and a branching yield of 90% for the radical channel (R9b): The alkoxy radicals formed in (R9b) will, in the presence of O_2, be rapidly transformed into formic acid and HO_2 radicals. Owing to the high yield of (R9b), the radical-recycling rate is much higher than that of (R3), so the impact on the radical loss at longer timescales will be less important. However, this reaction, if taking place at a noticeable rate on the timescale for establishing equilibrium (R1), could have an impact on the apparent HO_2 equilibrium constant: The adduct would act as a "reservoir" for HO_2 radicals, and the apparent HO_2 equilibrium concentration would increase with increasing initial radical concentration, just as observed in our experiments.

Therefore, experiments were performed at 297 K at nine different initial CH_2O and HO_2 concentrations, some repeated several times (15 experiments total), and a more complete mechanism was employed to retrieve the rate and equilibrium constants by simulating HO_2 decay profiles for the entire set of experimental conditions. The mechanism used to simulate the HO_2 decay profiles at 297 K with a custom Labview-based program is listed in Table I.

The effects of the two secondary reactions (R3) and (R9) on the modeled HO_2 concentration time profiles are shown in Fig. 3 for an experiment with one of the highest initial HO_2 concentrations used in this work (2.7×10^{12} cm^{-3}). The left figure shows the impact of the branching ratio for the reaction between HO_2 radicals and the peroxy adduct (R3). Raising the radical recycling reaction path (R3c) to 50% (instead of 15 or 20% as recommended by Jenkin et al. [13] and Nguyen et al. [14]) leads to a higher apparent HO_2 equilibrium concentration (red line), whereas reducing the yield to 0% underestimates the HO_2 concentration. The black line shows our best fit, using the literature value for the branching ratio. A similar effect can be seen on the right graph, where the rate constant k_{9b} for the radical-recycling pathway of the peroxy radical self-reaction (R9) has been varied (keeping the chain-terminating rate constant k_{9a} fixed at 7×10^{-13} cm^3 molecule^{-1} s^{-1}). An increase in the rate constant k_{9b} by 3×10^{-12} cm^3 molecule^{-1} s^{-1} from a best fit value of 7×10^{-12} cm^3 molecule^{-1} s^{-1} (red line) leads to an increase in the modeled HO_2 equilibrium concentration, whereas reducing k_{9b} by 3×10^{-12} cm^3 molecule^{-1} s^{-1} (green line) leads to a lower HO_2 equilibrium concentration. For both reactions, the slope of the slow decay of HO_2 radicals on longer timescales is barely influenced: This is not surprising for (R9), because the nonradical recycling path of (R9) is negligible (10%), so the overall radical concentration is not influenced very much by this reaction, even at longer reaction times. One might expect reaction (R3) to have a larger effect on the long-time decay of HO_2 radicals, since the major product pathway leads to radical loss. The biexponential fits such as shown in Fig. 1 or 2 do confirm a slight increase in the slow decay rate with increasing radical concentration; however, our initial radical concentrations were too low for the slow HO_2 decay to be sensitive to the branching ratio and the rate constant of (R3).

We systematically fitted all experiments at 297 K, using the literature values of the rate constants and branching ratios as initial starting parameters. We found that the HO_2 decay profiles could be fitted more consistently, i.e., with the same equilibrium constant, over the full range of initial CH_2O and radical concentrations, when the rate constant of (R9) was slightly increased above the only rate constant available in the literature (an increase from 6.06 to 7.7×10^{-12} cm^3 s^{-1}) while still keeping the yield for channel (R9a) at 10%. Additional slow diffusion terms were needed to fit the long-time decays. The final fitted values for the rate constants k_1, k_{-1}, and the equilibrium constant K_1 at 297 K are given in Table II.

Temperature Dependence of the Equilibrium Constant for the Reaction of HO_2 with CH_2O

The equilibrium constant for (R1) has been measured at four different temperatures in a small temperature

Table I Full Reaction Mechanism Used for the Simulation of the HO_2 Decays in the Presence of CH_2O at 297 K

Reaction	Equation	k (cm^3 $molecule^{-1}$ s^{-1})	Reference
$CH_2O + HO_2 \rightarrow HOCH_2O_2$	(R1)	$(3.3 \pm 0.6) \times 10^{-14}$	This work
$HOCH_2O_2 \rightarrow CH_2O + HO_2$	(R−1)	(55 ± 5) s^{-1}	This work
$HOCH_2O_2 + HO_2 \rightarrow$ Product	(R3a+b)	9.6×10^{-12}	[13] and [14]
$\rightarrow OH + HOCH_2O + O_2$	(R3c)	2.4×10^{-12}	
$HOCH_2O + O_2 \rightarrow HCOOH + HO_2$	(R4)	3.5×10^{-14}	[13]
$HCO + O_2 \rightarrow HO_2 + CO$	(R5)	5.2×10^{-12}	[17]
$H + O_2 \rightarrow HO_2$	(R6)	2.95×10^{-14}	[28]
$OH + CH_2O \rightarrow H_2O + CHO$	(R7)	8.5×10^{-12}	[38]
$OH + H_2O_2 \rightarrow HO_2 + H_2O$	(R8)	1.7×10^{-12}	[38]
$2HOCH_2O_2 \rightarrow$ Products	(R9a)	$(7 \pm 1) \times 10^{-13}$	This work
$\rightarrow 2HOCH_2O + O_2$	(R9b)	$(7 \pm 1) \times 10^{-12}$	
$2HO_2 \rightarrow H_2O_2 + O_2$	(R10)	1.7×10^{-12}	[38]
$HO_2 \rightarrow$ Diffusion	(R11)	7 s^{-1}	This work
$HOCH_2O_2 \rightarrow$ Diffusion	(R12)	6 s^{-1}	This work

Error for k_{-1} and k_9 is uncertainty from fitting. Error for k_1 is estimated from uncertainty in the CH_2O concentration.

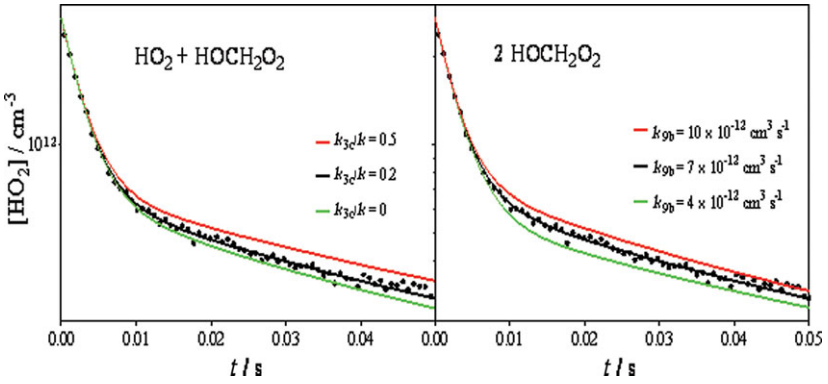

Figure 3 Impact of secondary chemistry on HO_2 profiles, $[CH_2O]_0 = 7.2 \times 10^{15}$ cm^{-3}, photolysis fluence 76 mJ cm^{-2}. Left graph, impact of (R3). Black line with the rate constants and branching ratios such as shown in Table II, red (upper) line $k_{3c}/k_3 = 0.5$, and green (lower) line $k_{3c}/k_3 = 0$. Right graph: impact of (R9): black line with the rate constants and branching ratios such as shown in Table II, red (upper) line $k_{9b} = 10 \times 10^{-12}$ $cm^3 molecule^{-1}$ s^{-1}, and green (lower) line $k_{9b} = 4 \times 10^{-12}$ cm^3 $molecule^{-1}$ s^{-1}.

Table II Reaction Parameters K_1, k_1, and k_{-1} as a Function of Temperature, Obtained by Fitting the HO_2 Concentration Time Profiles to the Full Model of Table I

T (K)	Number of Experiments	k_1 (cm^3 $molecule^{-1}$ s^{-1})	k_{-1} (s^{-1})	K_1 (molecule $^{-1}$ cm^3)
(292 ± 1)	9	$(3.4 \pm 0.7) \times 10^{-14}$	35 ± 3	$(9.7 \pm 1.9) \times 10^{-16}$
(297 ± 1)	15	$(3.3 \pm 0.6) \times 10^{-14}$	55 ± 5	$(6.0 \pm 1.8) \times 10^{-16}$
(303 ± 1)	9	$(3.1 \pm 0.6) \times 10^{-14}$	90 ± 10	$(3.4 \pm 1.0) \times 10^{-16}$
(306 ± 1)	12	$(3.0 \pm 0.6) \times 10^{-14}$	150 ± 20	$(2.0 \pm 0.6) \times 10^{-16}$

k_1 has been kept constant during fitting. Errors for k_1 are estimated 20% from uncertainty in the CH_2O concentration. Error for k_{-1} represents the range necessary to best reproduce HO_2 profiles from all experiments at a given temperature and thus includes the uncertainty in the temperature measurement. Errors for K_1 are the sum of both errors.

range (292–306 K). Experiments such as described in the above paragraph for 297 K were repeated for the three other temperatures, using a range of CH_2O concentrations and photolysis fluences at each temperature. The overall temperature range was limited at the lower end by the experimental setup, i.e., the photolysis reactor could not be cooled, and at the upper end by the highest achievable CH_2O concentration. At higher temperatures, the equilibrium HO_2 concentration increases (F_{fast} becomes small), i.e., the decay of

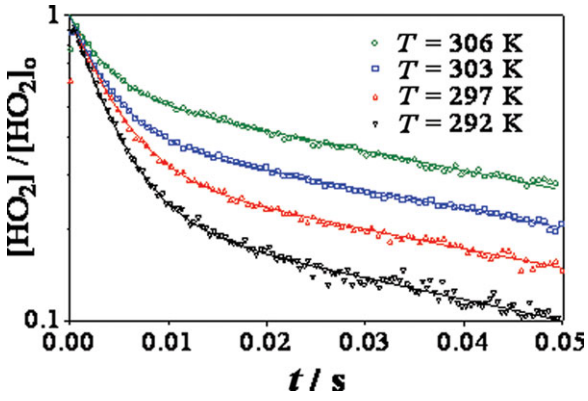

Figure 4 Normalized HO_2 concentration–time profiles as a function of reaction temperature. The initial CH_2O concentration was around 5×10^{15} cm^{-3}, and photolysis fluence was around 75 mJ cm^{-2}. The initial HO_2 concentration has been normalized and was around 2.5×10^{12} cm^{-3}.

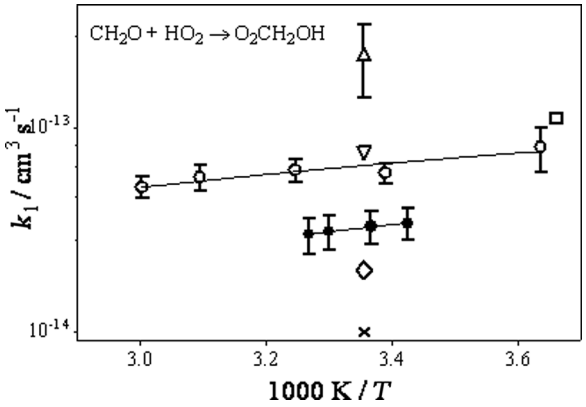

Figure 5 Rate constants for the forward reaction k_1: Δ, Morrison and Heicklen [6]; □, Barnes et al. [4] ∇, McAdam et al., [48] ◊, Thrush et al. [49]; ×, Su et al. [1] o, Veyret et al. [7] •, this work (error bars for this work represent 20%).

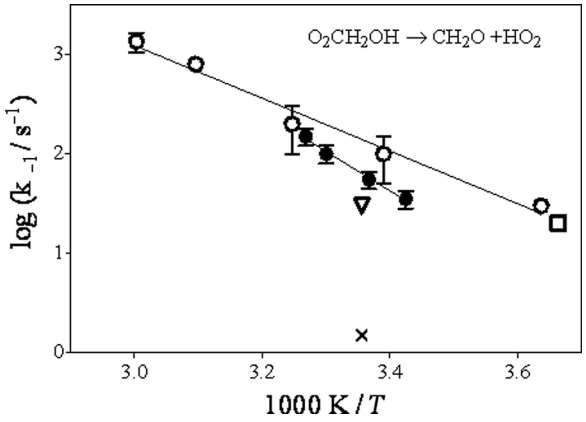

Figure 6 Rate constants for the back reaction k_{-1}; same symbols as in Fig. 5 (error bars for this work represent 20%).

HO_2 radicals becomes very small even at the maximum formaldehyde concentration, too small to allow for a clean separation between the two decays.

The normalized time profiles of the HO_2 concentration for experiments using similar CH_2O concentrations are shown for all four temperatures in Fig. 4. A strong dependence on the temperature can be observed. We simulated the time profiles using the mechanism in Table I, now adjusting only the rate constants for the equilibrium reaction (R1). The rate constants deduced from this procedure are shown in Table II: Error bars for k_{-1} represent the range of rate constants that were necessary to fit consistently the profiles for all experimental conditions at the same temperature, whereas the error bars for k_1 represent an estimated error of 20% on the CH_2O concentration. Only slight adjustments of the rate constant for the back reaction k_{-1} were needed to obtain good agreement between the simulations using the model in Table I and the HO_2 concentration–time profiles under all experimental conditions. The rate constant for the forward reaction was kept constant at a given temperature, and a slight negative temperature dependence for k_1 was obtained, in good agreement with Veyret et al. [7].

DISCUSSION

The rate coefficients and equilibrium constant for the reaction $HO_2 + CH_2O$ (R1) have been measured several times in the past, and all available data are summarized in Figs. 5, 6, and 7 for k_1, k_{-1} and K_1, respectively. Several results are available at around room temperature, but are scattered by more than one order of magnitude for the rate constant of both the forward and back reactions. Only one group has carried out a temperature-dependent study on the kinetics of this equilibrium [7], and their results are in excellent agreement with the only study at lower temperature [4]. Zabel et al. [5] reported only the temperature-dependent equilibrium constant but no kinetics; their result for K_1 is in poor agreement with both Burrows et al. [12] and Veyret et al. [7].

The temperature-dependent rate coefficients and equilibrium constant obtained in the current study for reaction (R1) are summarized in Table II and are presented together with the available data from the literature in Figs. 5–7. Unfortunately, the temperature range accessible in our experimental setup is rather limited, and with only two degrees of freedom (four data points for two variables) the derived ΔH°(297 K)

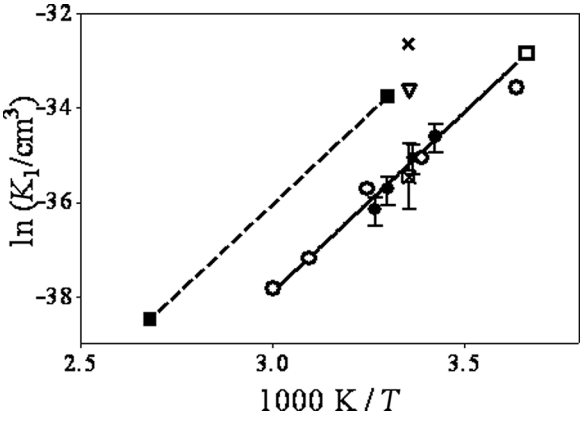

Figure 7 Equilibrium constant as a function of temperature. The same symbols as in Fig. 5; ■, Zabel et al. [5] □, Burrows et al. [12]. The full line is the IUPAC recommendation for the temperature dependence of the equilibrium constant. Error bars for this work represent 30% uncertainties.

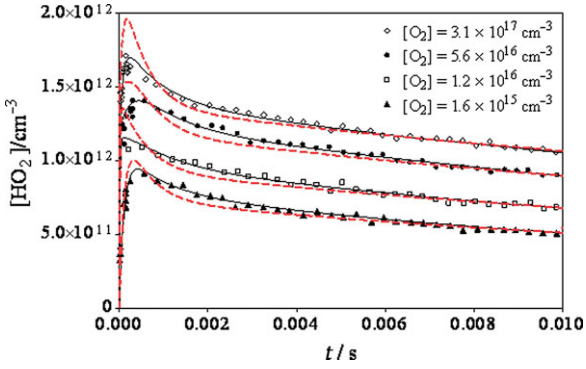

Figure 8 HO_2 concentration–time profile following the 248-nm photolysis (25 mJ cm^{-2}) of 1.67×10^{16} cm^{-3} CH_3CHO with $[O_2] = 5.6 \times 10^{16}$ cm^{-3}, full line same as Figs. 9 and 10. Upper, black dashed line shows the concentration–time profile for the adduct (R2), and lower colored dashed lines show different reaction products for the major HO_2 loss reactions.

and $\Delta S^{\circ}(297\ \mathrm{K})$ would have unreasonably high uncertainties. However, as can be seen from Fig. 7, both the absolute values and the temperature dependence of the equilibrium constant $K_1(T)$ are in excellent agreement with the earlier work of Veyret et al. [7] and Burrows et al. [12]. Our results are also consistent with the lower temperature determination of Barnes et al. [4]. In the resulting van t'Hoff plot as shown in Fig. 7, the current results fall directly on the line recommended by the IUPAC panel [17]. The reported exothermicity agrees well with theoretical predictions for the binding energy of the peroxy radical adduct $HOCH_2O_2$ predicted by ab initio calculations [8].

Arrhenius expressions for both rate constants are given by

$$k_1 = (3.7 \pm 0.7) \times 10^{-15} \exp(637/T)\ \mathrm{cm^3\ molecule^{-1}\ s^{-1}}$$

$$k_{-1} = (1.4 \pm 0.3) \times 10^{15} \exp(-9160/T)\ \mathrm{s^{-1}}$$

Error bars in the preexponential factor are estimated to be 20%, corresponding to the uncertainty in the determination of the CH_2O concentration. Again, these expressions are only valid over a limited temperature range and the small number of points indicates that the Arrhenius parameters should be treated with caution. The forward rate k_1 lies in the midst of the range of previously observed rates. It can be seen from Figs. 5 and 6 that the temperature dependences of both rate constants agree reasonably well with the only available temperature-dependent determinations by Veyret et al. [7]; however, the absolute values of both rate constants are roughly a factor of 2 slower.

A possible explanation for this disagreement might come from the difference in pressures. Veyret et al. [7] have carried out their experiments at pressures between 85 and 170 Torr N_2, whereas the total pressure in this work was only 50 Torr He. Even though Veyret et al. did not observe any pressure dependence of the rate constant, it is possible that the reaction might be in the falloff range at 50 Torr He. To estimate the possible impact of the falloff on the rate constant under our conditions, the reaction of CH_2O with HO_2 can be compared with the reaction of a species of comparable size. Propoxy radicals have, with four heavy atoms, a comparable falloff behavior and the decomposition of *i*-propoxy radicals has been studied over a large pressure range [35]. Veyret et al. worked in N_2, whereas our study was carried out in He, which has a collisional relaxation efficiency that is typically 60% of N_2 [36,37]. Comparison with the *i*-propoxy decomposition suggests that a factor of 2 for the decomposition rate constant of $HOCH_2O_2$ between 50 Torr He and 85 Torr N_2 is conceivable. However, it would have been expected that Veyret et al. would have also observed a pressure effect, because the reaction is not expected to be at the high-pressure limit at 85 Torr N_2.

Equilibrium Constant for the Reaction of HO_2 with CH_3CHO

Typical HO_2 concentration–time profiles following the 248-nm photolysis of acetaldehyde at different O_2 concentrations are shown in Fig. 8. At the lowest O_2

Table III Full Reaction Mechanism Used for the Simulation of the HO_2 decays at 294 K for (R2) plus (R5), (R6), (R10), and (R11) from Table I

Reaction	Equation	k (cm^3 $molecule^{-1}$ s^{-1})	Reference
$CH_3CHO + h\nu \rightarrow CH_3 + HCO$	(R13)	$\phi = 0.3$	Estimated from [21]
$\rightarrow CH_4 + CO$		$\phi = 0.6$	
$\rightarrow CH_3CO + H$		$\phi = 0.1$	
$CH_3CHO + HO_2 \rightarrow CH_3CH(OH)O_2$	(R2)	$(1.5 \pm 0.75) \times 10^{-14}$	This work
$CH_3CH(OH)O_2 \rightarrow CH_3OCHO + HO_2$	(R-2)	$900 \pm 450\ s^{-1}$	This work
$H + CH_3CHO \rightarrow H_2 + CH_3CO$	(R14)	1.1×10^{-13}	[39]
$CH_3 + CH_3 \rightarrow C_2H_6$	(R15)	5.5×10^{-11}	[40]
$CH_3 + O_2$ (+M) $\rightarrow CH_3O_2$ + (M)	(R16)	$1.6\ 10^{-13}$	[41,42]
$CH_3 + HO_2 \rightarrow CH_3O + OH$	(R17)	2.2×10^{-11}	Estimated from [43,44]
$\rightarrow CH_4 + O_2$		1.0×10^{-11}	
$CH_3O_2 + HO_2 \rightarrow$ products	(R18)	5.2×10^{-12}	[38]
$CH_3O_2 + CH_3O_2 \rightarrow 2\ CH_3O + O_2$	(R19)	1.3×10^{-13}	[17]
$\rightarrow$ Products		2.2×10^{-13}	
$CH_3O + O_2 \rightarrow CH_2O + HO_2$	(R20)	1.9×10^{-15}	[17]
$CH_3O + CH_3CHO \rightarrow CH_3CO + CH_3OH$	(R21)	7.0×10^{-14}	[45]
$CH_3CO + O_2 \rightarrow CH_3C(O)O_2$	(R22)	2.5×10^{-12}	[46]
$\rightarrow$ OH + products		1.05×10^{-12}	
$CH_3C(O)O_2 + HO_2 \rightarrow CH_3 + CO_2 + O_2 + OH$	(R23)	6.16×10^{-12}	[17][a]
$\rightarrow$ products		7.57×10^{-12}	
$2\ CH_3C(O)O_2 \rightarrow 2\ CH_3 + 2\ CO_2 + O_2$	(R24)	1.6×10^{-11}	[17]
$CH_3C(O)O_2 + CH_3O_2 \rightarrow CH_3O + CH_3 + CO_2 + O_2$	(R25)	9.9×10^{-12}	[17]
$\rightarrow$ products		1.1×10^{-12}	
$OH + CH_3CHO \rightarrow H_2O + CH_3CO$	(R26)	1.5×10^{-11}	[38]
$CH_3CH(OH)O_2 \rightarrow$ Diffusion	(R27)	$5\ s^{-1}$	This work

[a]A recent work of Taraborrelli et al. [47] gives higher overall rate constant (+40%) and higher yield for radical channel (70%) for (R23): This reaction has only small impact on HO_2 decay at long reaction times and no impact on K_2; therefore, we have used the latest IUPAC recommendations.

concentration (▲), HO_2 radicals are mainly generated from (R5), because the reaction of H-atoms with O_2 (R6) is too slow to compete with the reaction of H-atoms with CH_3CHO (R14). At the higher O_2 concentrations, (R5) is not resolved anymore and HO_2 radicals from (R5) are formed immediately on the timescale of the experiments. With increasing O_2 concentrations (• and ◊), reaction (R6) becomes fast enough to compete with (R14) and H atoms are also converted partially to HO_2 radicals: therefore, the total HO_2 concentration increases with increasing O_2 concentration for a given CH_3CHO concentration and photolysis energy. At typical radical concentrations (few 10^{12} cm^{-3}), HO_2 losses through radical–radical reactions (R17, R18, R23 in Table III) are rather slow and the decay of HO_2 radicals during the first milliseconds is mostly governed by establishing the equilibrium between CH_3CHO and HO_2. Figure 9 demonstrates this by showing different traces for one of the experiments from Fig. 8: The concentration–time profiles of the peroxy adduct such as obtained by the model is plotted as a dashed line together with the products from other major HO_2 loss reactions (R11, R18, and R23). The decay at longer reaction times is influenced by the diffusion of radicals out of the observation volume but also by some other reactions. The model used for simulating the profiles in Figs. 8 and 10 is shown in Table III. Reactions of the adduct $CH_3CH(OH)O_2$ with itself, HO_2, CH_3O_2, or $CH_3C(O)O_2$ have been included into the model such as proposed by Tomas et al. [20] (not shown in Table III), but do have only a very minor impact on the HO_2 profiles.

The equilibrium constant of the reaction between CH_3CHO and HO_2 is roughly 40 times smaller than the corresponding reaction of HO_2 with CH_2O, and hence the HO_2 loss due to the equilibrium is less important for comparable aldehyde concentrations, resulting in a lower sensitivity of HO_2 profiles for the equilibrium constant. Figure 8 shows the influence of the equilibrium constant on the shape of the HO_2 profile for the highest CH_3CHO concentration: The full lines have been obtained by fixing the rate constant for the forward reaction k_{-2} to the value proposed by Moortgat et al. [21] (1.5×10^{-14} cm^3 $molecule^{-1}$ s^{-1}) and adjusting the rate constant for the back reaction k_2: The best agreement with experimental HO_2 profiles is

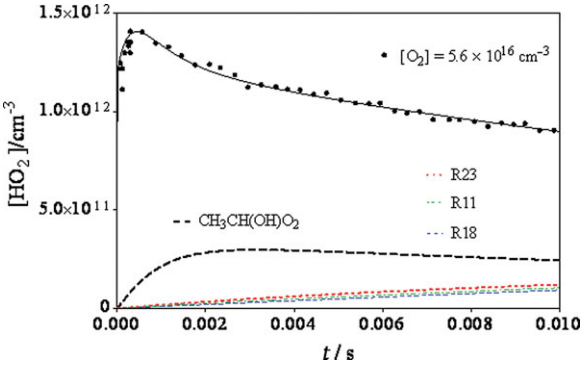

Figure 9 HO_2 concentration–time profiles following the 248-nm photolysis (25 mJ cm^{-2}) of 1.67×10^{16} cm^{-3} CH_3CHO in the presence of four different O_2 concentrations. The full lines represent the model as shown in Table III with $K_2 = 1.66 \times 10^{-17}$ cm^3 $molecule^{-1}$, and the red dashed red lines represent the model using $K_2 = 3.2 \times 10^{-17}$ cm^3 $molecule^{-1}$ from Tomas et al. [20]: Initial radical concentrations have been increased by up to 20% to best reproduce the HO_2 equilibrium concentration at longer reaction times.

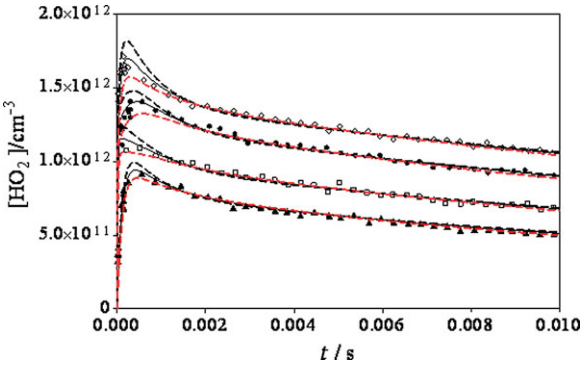

Figure 10 Same experiments as in Fig. 8: the full line model from Table III, dashed black lines $k_{17} = 2.25 \pm 10^{-14}$ cm^3 $molecule^{-1}$ s^{-1}, dashed red line $k_{17} = 0.75 \pm 10^{-14}$ cm^3 $molecule^{-1}$ s^{-1}, $k_{-17} = 900$ s^{-1} in all cases. Initial radical concentrations have been varied by maximal ±13% to best reproduce the equilibrium concentration at longer reaction times.

obtained with $k_{-2} = 900$ s^{-1}, leading to an equilibrium constant of $K_2 = 1.7 \times 10^{-17}$ $molecule^{-1}$ cm^3. The dashed red lines in Fig. 8 have been obtained by applying the rate and equilibrium constants from Tomas et al. [20]. To reproduce the HO_2 equilibrium concentration at longer reaction times, the initial radical concentration has been increased by a maximum of 23%, well within the uncertainty of the absolute HO_2 concentration (mainly determined by the quantum yield of CH_3CHO photolysis). However, using the equilibrium constant from Tomas et al., the model is in very poor agreement with the HO_2 profiles at short reaction times: The decay of the HO_2 concentration is too fast. The equilibrium constant such as obtained by Tomas et al. is based on a complex model including several peroxy cross-reactions, for which rate constants and product yields have changed since publication of [17].

To demonstrate the sensitivity of the HO_2 profiles to the equilibrium constant, the same experiments are shown again in Fig. 10: The dashed lines have been obtained by varying the rate constant for the forward reaction k_2 by ±50% while keeping the rate constant for the back reaction, k_{-2}, at 900 s^{-1}, i.e., varying the equilibrium constant by ±50%. Again, the initial radical concentrations have been adjusted to best reproduce the equilibrium HO_2 concentration at longer reaction times: The maximum change needed for all conditions was 13%, well within the uncertainty of the absolute HO_2 concentration. However, it can be seen that the HO_2 profiles at short reaction times are not well reproduced by this variation and from this we estimate the uncertainty on the equilibrium constant to be 30%: $K_2 = (1.7 \pm 0.5) \times 10^{-17}$ $molecule^{-1}$ cm^3. The sensitivity of the experiment for the individual rate constants is poorer: HO_2 profiles can still be reasonably well reproduced by varying the rate constant for the forward reaction by ±50% while adjusting at the same time the rate constant for the back reaction:

$$k_2 = (1.5 \pm 0.75) \times 10^{-14}\ \text{cm}^3\ \text{molecule}^{-1}\ \text{s}^{-1}$$

$$k_{-2} = (900 \pm 450)\ \text{s}^{-1}$$

It is clear that experiments with higher CH_3CHO concentration would increase the sensitivity of the HO_2 profiles to the equilibrium (R2) and thus decrease the uncertainty on the rate and equilibrium constants. This, however, is difficult because CH_3CHO tends to polymerize at higher concentrations. Experiments at lower temperature would be an even better means to study this equilibrium reaction more precisely. Unfortunately, our experimental setup does not allow the reactor to be cooled.

The improved equilibrium constant for reaction (R2) has no impact on atmospheric chemistry and especially will not be able to explain the disagreement between recent observations and model [15]. However, it might have some importance in laboratory studies, where higher concentrations are used.

CONCLUSIONS

The reactions of HO_2 radicals with CH_2O and CH_3CHO have been studied at 50 Torr helium through

direct, selective measurement of HO_2 radicals. For CH_2O, the equilibrium constant is found to be in excellent agreement with the literature data over the entire temperature range (292–306 K) whereas the rate constants of the forward and back reactions were found to be two times lower than the literature data, possibly due to falloff effects. The HO_2 time profiles were more consistently reproduced when the rate constant for the self-reaction of the adduct, $HOCH_2O_2 + HOCH_2O_2$, was slightly increased from 6.1×10^{-12} to 7.7×10^{-12} cm^3 $molecule^{-1}$ s^{-1} compared to the only available literature value [12]. For CH_3CHO, the equilibrium constant is smaller compared to CH_2O and the sensitivity of the HO_2 profiles is lower. The equilibrium constant at 294 K has been found $(1.7 \pm 0.5) \times 10^{-17}$ $molecule^{-1}$ cm^3, in poor agreement with earlier measurements [20], but in good agreement with a recent, more indirect estimation [21].

The laboratory participates in the Institut de Recherche en ENvironnement Industriel (IRENI), which is financed by Région Nord Pas-de-Calais, the Ministère de l'Enseignement Supérieur et de la Recherche, the CNRS, and European Regional Development Fund (ERDF). This project was supported by the French ANR agency under contract no. ANR−11-LabEx-0005–01 CaPPA (Chemical and Physical Properties of the Atmosphere) and by the CNRS through the French–German program "ATMOCHEM." MO acknowledges support of the Upper Atmospheric Research Program (UARP) of the U.S. National Aeronautics and Space Administration (NASA) for grant NNX12AE01G, and IRENI for a visiting professorship.

BIBLIOGRAPHY

1. Su, F.; Calvert, J. G.; Shaw, J. H. J Phys Chem 1979, 83, 3185–3191.
2. Niki, H.; Maker, P. D.; Savage, C. M.; Breitenbach, L. P. Chem Phys Lett 1980, 72, 71–73.
3. Veyret, B.; Rayez, J. C.; Lesclaux, R. J Phys Chem 1982, 86, 3424–3430.
4. Barnes, I.; Becker, K. H.; Fink, E. H.; Reimer, A.; Zabel, F.; Niki, H. Chem Phys Lett 1985, 115, 1–8.
5. Zabel, F.; Sahetchian, K. A.; Chachaty, C. Chem Phys Lett 1987, 134, 433–437.
6. Morrison, B. M.; Heicklen, J. J Photochem 1981, 15, 131–145.
7. Veyret, B.; Lesclaux, R.; Rayez, M. T.; Rayez, J. C.; Cox, R. A.; Moortgat, G. K. J Phys Chem 1989, 93, 2368–2374.
8. Hermans, I.; Müller, J.-F.; Nguyen, T. L.; Jacobs, P. A.; Peeters, J. J Phys Chem A 2005, 109, 4303–4311.
9. Anglada, J. M.; Domingo, V. M. J Phys Chem A 2005, 109, 10786–10794.
10. Delcey, M. G.; Lindh, R.; Linguerri, R.; Hochlaf, M.; Francisco, J. S. J Chem Phys 2013, 138, 021105.
11. Sprague, M. K.; Mertens, L. A.; Widgren, H. N.; Okumura, M.; Sander, S. P. J Phys Chem A 2013, doi: 10.1021/jp400390y.
12. Burrows, J. P.; Moortgat, G. K.; Tyndall, G. S.; Cox, R. A.; Jenkin, M. E.; Hayman, G. D.; Veyret, B. J Phys Chem 1989, 93, 2375–2382.
13. Jenkin, M. E.; Hurley, M. D.; Wallington, T. J. Phys Chem Chem Phys 2007, 9, 3149–3162.
14. Nguyen, T. L.; Vereecken, L.; Peeters, J. Z Phys Chem 2010, 224, 1081–1093.
15. Read, K. R.; Carpenter, L.; Arnold, S. R.; Beale, R.; Nightingale, P.; Hopkins, J. R.; Lewis, A. C.; Lee, J. D.; Mendes, L.; Pickering, S. J. Environ Sci Technol 2012, 46, 11028–11039.
16. Lamarque, J.-F.; Emmons, L. K.; Hess, P. G.; Kinnison, D. E.; Tilmes, S.; Vitt, F.; Heald, C. L.; Holland, E. A.; Lauritzen, P. H.; Neu, J.; Orlando, J. J.; Rasch, P. J.; Tyndall, G. K. Geosci Model Dev 2012, 5, 369–411.
17. Atkinson, R.; Baulch, D. L.; Cox, R. A.; Crowley, J. N.; Hampson, R. F.; Hynes, R. G.; Jenkin, M. E.; Rossi M. J.; Troe, J.; Atmos Chem Phys 2006, 6, 3625–4055.
18. Moortgat, G. K.; Cox, R. A.; Schuster, G.; Burrows, J. P.; Tyndall, G. S. J Chem Soc, Faraday Trans 1989, 85, 809–829.
19. Crawford, M. A.; Wallington, T. J.; Szente, J. J.; Maricq, M. M.; Francisco, J. S. J Phys Chem A 1999, 103, 365–378.
20. Tomas, A.; Villenave, E.; Lesclaux, R. J Phys Chem A 2001, 105, 3505–3514.
21. Moortgat, G. K.; Meyrahn, H.; Warneck, P. Chem Phys Chem 2010, 11, 3896–3908.
22. Thiebaud, J.; Fittschen, C. App Phys B: Lasers Opt 2006, 85, 383–389.
23. Parker, A.; Jain, C.; Schoemaecker, C.; Szriftgiser, P.; Votava, O.; Fittschen, C. App Phys B: Lasers Opt 2011, 103, 725–733.
24. Votava, O.; Masat, M.; Parker, A. E.; Jain, C.; Fittschen, C. Rev Sci Instrum 2012, 83, 043110.
25. Morajkar, P.; Schoemaecker, C.; Fittschen, C. J Mol Spectrosc 2012, 281, 18–23.
26. Thiebaud, J.; Crunaire, S.; Fittschen, C. J Phys Chem A 2007, 111, 6959–6966.
27. Smith, G. D.; Molina, L. T.; Molina, M. J. J Phys Chem A 2002, 106, 1233–1240.
28. Fernandes, R. X.; Luther, K.; Troe, J.; Ushakov, V. G. Phys Chem Chem Phys 2008, 10, 4313–4321.
29. Baulch, D. L.; Cobos, C. J.; Cox, R. A.; Frank, P.; Hayman, G.; Just, T.; Kerr, J. A.; Murrells, T.; Pilling, M. J.; Troe, J.; Walker, R. W.; Warnatz, J. J Phys Chem Ref Data 1994, 23, 847–1033.
30. Thiebaud, J.; Aluculesei, A.; Fittschen, C. J Chem Phys 2007, 126, 186101.
31. Dillon, T. J.; Pozzer, A.; Vereecken, L.; Crowley, J. N.; Lelieveld, J. Atmos Chem Phys 2012, 12, 1339–1351.
32. Grieman, F. J.; Noell, A. C.; Davis-Van Atta, C.; Okumura, M.; Sander, S. P. J Phys Chem A 2011, 115, 10527–10538.
33. Hermans, I.; Nguyen, T. L.; Jacobs, P. A.; Peeters, J. J Am Chem Soc 2004, 126, 9908–9909.

34. Cours, T.; Canneaux, S.; Bohr, F. Int J Quantum Chem 2007, 107, 1344–1354.
35. Devolder, P.; Fittschen, C.; Frenzel, A.; Hippler, H.; Poskrebyshev, G.; Striebel, F.; Viskolcz, B. Phys Chem Chem Phys 1999, 1, 675–681.
36. Hippler, H.; Krasteva, N.; Nasterlack, S.; Striebel, F. J Phys Chem A 2006, 110, 6781–6788.
37. Dames, E. E.; Golden, D. M. J Phys Chem A 2013, doi: 10.1021/jp404836m.
38. Atkinson, R.; Baulch, D. L.; Cox, R. A.; Crowley, J. N.; Hampson, R. F.; Hynes, R. G.; Jenkin, M. E.; Rossi, M. J.; Troe, J. Atmos Chem Phys 2004, 4, 1461–1738.
39. Ohmori, K.; Miyoshi, A.; Matsui, H.; Washida, N. J Phys Chem 1990, 94, 3253–3255.
40. Wang, B.; Hou, H.; Yoder, L. M.; Muckerman, J. T.; Fockenberg, C. J Phys Chem A 2003, 107, 11414–11426.
41. Selzer, E. A.; Bayes, K. D. J Phys Chem 1983, 87, 392–394.
42. Fernandes, R. X.; Luther, K.; Troe, J. J Phys Chem A 2006, 110, 4442–4449.
43. Jasper, A. W.; Klippenstein, S. J.; Harding, L. B. Proc Combust Inst 2009, 32, 279–286.
44. Hong, Z.; Davidson, D. F.; Lam, K.-Y.; Hanson, R. K. Combust Flame 2012, 159, 3007–3013.
45. Fittschen, C.; Delcroix, B.; Gomez, N.; Devolder, P. J Chim Phys Phys-Chim Biol 1998, 95, 2129–2142.
46. Carr, S. A.; Baeza-Romero, M. T.; Blitz, M. A.; Pilling, M. J.; Heard, D. E.; Seakins, P. W. Chem Phys Lett 2007, 445, 108–112.
47. Taraborrelli, D.; Lawrence, M. G.; Crowley, J. N.; Dillon, T. J.; Gromov, S.; Grosz, C. B. M.; Vereecken, L.; Lelieveld, J. Nat Geosci 2012, 5, 190–193.
48. McAdam, K.; Veyret, B.; Lesclaux, R. Chem Phys Lett 1987, 133, 39–44.
49. Thrush, B. A.; Tyndall, G. S. J Chem Soc, Faraday Trans 1982, 78, 1469–1475.